JGP Journal of General Physiology

RESEARCH ARTICLE

Anoctamin 5/TMEM16E facilitates muscle precursor cell fusion

Jarred M. Whitlock, Kuai Yu, Yuan Yuan Cui, and H. Criss Hartzell

Limb-girdle muscular dystrophy type 2L (LGMD2L) is a myopathy arising from mutations in *ANO5*; however, information about the contribution of ANO5 to muscle physiology is lacking. To explain the role of ANO5 in LGMD2L, we previously hypothesized that ANO5-mediated phospholipid scrambling facilitates cell–cell fusion of mononucleated muscle progenitor cells (MPCs), which is required for muscle repair. Here, we show that heterologous overexpression of ANO5 confers Ca^{2+}-dependent phospholipid scrambling to HEK-293 cells and that scrambling is associated with the simultaneous development of a nonselective ionic current. MPCs isolated from adult *Ano5*$^{-/-}$ mice exhibit defective cell fusion in culture and produce muscle fibers with significantly fewer nuclei compared with controls. This defective fusion is associated with a decrease of Ca^{2+}-dependent phosphatidylserine exposure on the surface of *Ano5*$^{-/-}$ MPCs and a decrease in the amplitude of Ca^{2+}-dependent outwardly rectifying ionic currents. Viral introduction of *ANO5* in *Ano5*$^{-/-}$ MPCs restores MPC fusion competence, ANO5-dependent phospholipid scrambling, and Ca^{2+}-dependent outwardly rectifying ionic currents. *ANO5*-rescued MPCs produce myotubes having numbers of nuclei similar to wild-type controls. These data suggest that ANO5-mediated phospholipid scrambling or ionic currents play an important role in muscle repair.

Introduction

During the past several decades, advances in molecular genetics have greatly accelerated our capacity to identify variants linked to genetic diseases. However, elucidating the processes that lead to pathology lags significantly behind our diagnostic abilities. The limb-girdle muscular dystrophies (LGMDs) are a case in point. In the last decade, 15 new genes have been linked to LGMDs, but how mutations in these genes contribute to their associated diseases remains incompletely understood.

Muscular dystrophies encompass a heterogeneous group of pathologies characterized by progressive skeletal muscle weakness and atrophy. There are now at least 34 genes that have been linked to LGMDs that primarily affect hip or shoulder, girdle, and limb muscles. Here, we focus on LGMD type 2L (LGMD2L), an autosomal-recessive LGMD that is characterized by late onset (onset range, 11–50 yr) with myalgia that is commonly associated with exercise intolerance, progressive muscle weakness/atrophy, and elevated serum creatine kinase (Liewluck and Milone, 2018). LGMD2L was linked to mutations in *ANO5* (*TMEM16E*) in 2010 (Bolduc et al., 2010; Mahjneh et al., 2010; Hicks et al., 2011), but how ANO5 participates in muscle function remains a mystery.

Many LGMD genes encode proteins that are involved in maintaining muscle structural integrity. For example, the most common LGMDs, the α-dystroglycanopathies (10 LGMD2-linked genes), are caused by defects in proteins linking the muscle cytoskeleton to the extracellular matrix through the sarcolemma. When this support system is perturbed, it renders the muscle sarcolemma more susceptible to mechanical damage (Endo, 2015). Other LGMD genes, such as those encoding dysferlin (LGMD2B) and caveolin (LGMD1C), are thought to play roles in membrane repair (Bansal and Campbell, 2004; Corrotte et al., 2013). Because muscle is subjected to physical stress during activity, highly sophisticated processes exist to repair damage and regenerate injured muscle (Han and Campbell, 2007; Dumont et al., 2015). Previous work has suggested that mutations in ANO5 alter muscle repair processes (Jaiswal et al., 2007; Bolduc et al., 2010; Griffin et al., 2016). For example, we previously characterized an *Ano5*$^{-/-}$ knockout mouse that recapitulates many features of LGMD2L and demonstrated that this mouse exhibits defective muscle repair processes, both in vivo and in vitro (Griffin et al., 2016). One mechanism by which muscle fibers are repaired involves fusion of mononucleated muscle progenitor cells (MPCs) with damaged muscle. Just as multinucleated muscle fibers are formed during embryogenesis by the fusion of hundreds to thousands of MPCs (Abmayr and Pavlath, 2012), this process is recapitulated during muscle repair and regeneration as MPCs are recruited to fuse with and repair torn fibers or to

Department of Cell Biology, Emory University School of Medicine, Atlanta, GA.

Correspondence to H. Criss Hartzell: criss.hartzell@emory.edu.

form new muscle fibers (Collins et al., 2005; Glover and Brown, 2007; Gurevich et al., 2016).

The repair of multinucleated muscle fibers by fusion of mononucleated MPCs involves several steps, including proliferation and differentiation of fusion-competent cells, migration of cells to the site of fusion, recognition and adhesion of fusion-competent cells, and finally cell fusion. We suggest that ANO5 plays a role in regulating or coordinating this process during regenerative muscle repair.

Initially, it was thought that ANO5 was an ion channel because the founding members of the 10-gene ANO/TMEM16 family are Ca^{2+}-activated Cl^- channels (Caputo et al., 2008; Schroeder et al., 2008; Yang et al., 2008; Pedemonte and Galietta, 2014; Picollo et al., 2015; Whitlock and Hartzell, 2017). However, it is now recognized that many ANO paralogs are not Cl^- channels but have other functions, most notably Ca^{2+}-activated phospholipid scrambling (Ca^{2+}-PLS; Suzuki et al., 2010; Malvezzi et al., 2013; Brunner et al., 2014; Whitlock and Hartzell, 2017). ANO6 was the first ANO found to exhibit phospholipid scramblase (PLSase) activity, but more recently, two ANO homologues from fungi were found to be PLSases when purified and reconstituted into liposomes (Malvezzi et al., 2013; Brunner et al., 2014; Pelz et al., 2018). One of these scramblases has been crystallized (Brunner et al., 2014), which has greatly informed efforts to elucidate how it functions (Bethel and Grabe, 2016; Jiang et al., 2017). While initial reports suggested that ANO5 was not a PLSase (Suzuki et al., 2013), other evidence suggests that it might elicit Ca^{2+}-PLS in certain biological contexts (Gyobu et al., 2015). Moreover, recent evidence has suggested that ANO5-dependent PLS might play a role in the development of gnathodiaphyseal dysplasia (Di Zanni et al., 2018).

PLS is used by many cells as a means of cell–cell communication during a variety of biological processes, including cell fusion (Bevers and Williamson, 2010). The plasma membrane (PM) is composed of two lipid monolayers that exhibit tightly regulated asymmetric lipid organization, with the extracellular leaflet enriched in phosphatidylcholine and sphingomyelin and an intracellular leaflet enriched in phosphatidylserine (PtdSer), phosphatidylinositides, and phosphatidylethanolamine (reviewed in van Meer et al., 2008). When activated by increases in cytosolic Ca^{2+}, PLSases form a hydrophilic pathway through the membrane, facilitating the diffusion of polar lipid head groups nonselectively between membrane leaflets, resulting in the loss of leaflet asymmetry (Pomorski and Menon, 2006; Brunner et al., 2016). The loss of this asymmetry has a variety of biophysical consequences, including altered lipid packing and lateral pressure between lipid head groups (Whitlock and Hartzell, 2017). In addition, PLS exposes PtdSer and phosphatidylethanolamine to the extracellular face, where they are recognized by a variety of both soluble and membrane-bound receptors that elicit diverse intracellular signaling cascades in neighboring cells (Bevers and Williamson, 2016). PtdSer exposure via PLS is spatiotemporally linked to muscle fusion (van den Eijnde et al., 1997, 2001; Jeong and Conboy, 2011), both during development and regeneration, and it has been suggested that PtdSer exposure is a signal for cell–cell fusion. Several PtdSer receptors have recently been identified for their role in regulating the fusion of MPCs; Hochreiter-Hufford et al., 2013; Hamoud et al., 2014; Kim et al., 2016; Park et al., 2016).

Here we investigate the function of the ANO5/TMEM16E protein and explore how loss of *Ano5* affects muscle cell biology. We begin by studying the function of ANO5 in a heterologous expression system. We find that exogenous ANO5 confers Ca^{2+}-PLS to HEK-293 cells. Moreover, we find that ANO5-dependent Ca^{2+}-PLS is associated with the development of an ionic conductance. This conductance, like that described for ANO6 and the fungal ANO scramblases afTMEM16 and nhTMEM16 (Malvezzi et al., 2013; Yu et al., 2015; Lee et al., 2016), is ion nonselective. Next, we investigated the Ca^{2+}-PLS activity of fusogenic, primary MPCs and find that the loss of *Ano5* perturbs both the Ca^{2+}-dependent exposure of PtdSer and PLS-associated ionic currents. Introducing exogenous *ANO5* restores Ca^{2+}-PLS in *Ano5*$^{-/-}$ MPCs and rescues the coordination of the fusion in these cells producing muscle fibers with significantly increased myonuclear number. We believe this work suggests a role for ANO5-dependent Ca^{2+}-PLS in the coordination of proper MPC fusion to produce multinucleated skeletal muscle fibers.

Abstracts of this work have been published previously (Whitlock et al., 2015, 2016).

Materials and methods

Surface biotinylation

Surface proteins were covalently biotinylated by 0.5 mg/ml Sulfo-NHS-LC biotin (sulfosuccinimidyl-6-[biotin-amido]hexanoate, Pierce) for 40 min on ice. The reaction was quenched with 20 mM glycine for 30 min on ice. Protein lysates were collected in RIPA buffer (TEKNOVA) with protease inhibitors, and one-fifth soluble protein lysate was reserved to evaluate "total" protein. The remaining lysate was incubated with streptavidin-conjugated beads overnight at 4°C to capture biotinylated proteins. Total and biotinylated surface membrane protein pools were evaluated via Western blot.

Western blot

Steady-state protein levels were evaluated via SDS-PAGE followed by immunoblot. Antibodies used were mouse anti-ANO5 clone 85.1 (1:250, Q4KMQ2; UC-Davis Neuromab, Antibodies Inc.), mouse anti-FLAG (1:1,000, F1804; Sigma), anti-ANO6 (1:1,000, PA5-58610; Invitrogen), and mouse anti-GAPDH (1:1,000, MAB374; Millipore).

Cell culture

T-REx-293 cells (Invitrogen) or HEK293 cells (ATCC) were maintained in modified, high-glucose DMEM (supplemented with 10% FBS, 100 U/ml penicillin G, and 100 µg/ml streptomycin). Primary mouse myoblasts were isolated as described previously (Griffin et al., 2016) from 3-mo-old Ano5$^{-/-}$ or age matched wild-type C57BL/6J mice. Myoblasts were maintained in growth media (Ham's F10 media [Invitrogen] supplemented with 20% FBS, 5 ng/ml basic fibroblast growth factor, 100 U/ml penicillin G, and 100 µg/ml streptomycin) on bovine collagen–coated plates (Gibco).

cDNA constructs

mANO6 (Uniprot: Q6P9J9) was tagged on the C terminus with Clover fluorescent protein and inserted into the pcDNA5/TO

plasmid (Invitrogen). A codon-optimized cDNA for hANO5 (Uniprot: Q75V66) was synthesized by DNA2.0 (Newark, CA) and tagged on the C terminus with Clover or 3XFLAG and inserted into the pcDNA5/TO plasmid (Invitrogen). For designing chimeras, mANO1 and hANO5 cDNAs were aligned using MUSCLE (McWilliam et al., 2013). Chimeras were constructed using overlap extension PCR (Pont-Kingdon, 1997). Chimeras are named X-Y-X, where X is the ANO paralog template whose amino acids are replaced with the aligned amino acids from ANO paralog Y. For ANO151, amino acids 554–588 of ANO1 were replaced with amino acids 530–564 from ANO5, and for ANO515, amino acids 530–564 of ANO5 were replaced with amino acids 554–588 from ANO1. PCR primers were designed to engineer complementary overlapping sequences onto the junction-forming ends of PCR products that were subsequently assembled by PCR. PCR-based mutagenesis was used to generate mutations in one or a few amino acids. The protein coding region of all chimeras and mutants were sequenced. Plasmids were introduced into T-REx-293 cells using Lipofectamine 2000, and stable incorporation was selected using hygromycin B (Invitrogen) and blasticidin (Sigma) according to the manufacturer's protocol. Protein expression was induced by supplementing cell culture media with 2 µM tetracycline (Sigma) overnight.

PLS assay

PLS was assessed by live-cell imaging using the PtdSer binding proteins annexin V–Alexa Fluor 568 or LactC2-mCherry and –Clover, as described previously (Yu et al., 2015). Briefly, cells were washed in nominally Ca^{2+}-free PLS solution (140 mM NaCl, 5 mM KCl, 10 mM Tris-HCl, pH 7.4, mOsm 360 mM), treated for 5 min with PLS solution + 10 µM A23187, washed, and stimulated by the addition of Ca^{2+} (typically 5 mM). A23187 in nominally zero-Ca^{2+} depletes ER stores and activates store operated Ca^{2+} entry that elevates cytosolic Ca^{2+} upon addition of extracellular Ca^{2+}. PLS and simultaneous patch-clamp recording was conducted by elevating intracellular [Ca^{2+}] via the pipette solution as described previously (Yu et al., 2015).

MPC fusion assay

Primary MPCs were plated on entactin-collagen IV-laminin matrix (Millipore)–coated 12-well plates (Sigma) and allowed to adhere to the dish overnight in growth media. Cells were switched to differentiation medium (1 g/L glucose; DMEM), supplemented with 1% horse serum (Gibco) the following morning, and cultured for ∼36 h. Cells were fixed in 4% paraformaldehyde and stained with DAPI (Invitrogen) and Phalloidin (Invitrogen). Two collections of 3 × 3 overlapping images (total area per image = 5.49 mm^2) were taken at random of each well for each condition. Each collection of images was stitched together and evaluated for the number of fibers per nuclei represented using ImageJ cell counter.

Electrophysiology

Single cells expressing ANO5-Clover, ANO1-EGFP, or ANO6-EGFP were identified by fluorescence on a Zeiss Axiovert microscope and voltage-clamped using conventional whole-cell patch-clamp techniques with an EPC-7 (HEKA) or Axopatch 200A (Molecular Devices) amplifiers. Fire-polished borosilicate patch pipettes were 3–5 MΩ. Experiments were conducted at ambient temperature (24–26°C). Because liquid junction potentials calculated using pClamp were predicted to be <2 mV, no correction was made. Solutions had the following composition (in mM) as follows. Zero intracellular Ca^{2+}: 146 CsCl, 2 $MgCl_2$, 5 EGTA, 10 sucrose, 10 HEPES, pH 7.3, adjusted with NMDG; 20 µM intracellular Ca^{2+}: 146 CsCl, 2 $MgCl_2$, 5 Ca^{2+}-EGTA, 10 sucrose, 10 HEPES, pH 7.3, adjusted with NMDG; 0.2 mM intracellular Ca^{2+}: 0.2 $CaCl_2$ was added to the 20 µM Ca^{2+}solution; standard extracellular solution: 140 NaCl, 5 KCl, 2 $CaCl_2$,1 $MgCl_2$, 15 glucose, 10 HEPES, pH 7.4. For determining ionic selectivity, 140 mM NaCl in the standard extracellular solution was replaced with the indicated concentrations of NaCl, CsCl, or NMDG-Cl as indicated, and the internal solution contained (in mM) 150 NaCl (or CsCl), 1 $MgCl_2$, 5 Ca-EGTA, 0.2 $CaCl_2$, and 1 HEPES, pH 7.4. The osmolarity of each solution was adjusted to 300 mOsm by addition of mannitol. Relative permeabilities of cations relative to Cl^- were determined by measuring the changes in zero-current E_{rev} using the Goldman–Hodgkin–Katz equation when the concentration of extracellular ions were changed (dilution potential method) as previously described (Yu et al., 2012):

$$\Delta E_{rev} = 25.7 \ln[(X_0 + Cl_i{*}P_{Cl}/P_{Na})/(X_i + Cl_0{*}P_{Cl}/P_{Na})],$$

where X is the cation and ΔE_{rev} is the difference between E_{rev} with the test solution XCl and that observed with symmetrical solutions. MPCs were evaluated in the same manner as HEK cells with an intracellular solution composed of 146 mM CsCl, 2 mM $MgCl_2$, 5 mM Ca^{2+}-EGTA, 10 mM sucrose, 10 mM HEPES, and 0.2 mM $CaCl_2$ and an extracellular solution composed of 140 mM NaCl, 5 mM KCl, 2 mM $CaCl_2$,1 mM $MgCl_2$, 15 mM glucose, and 10 mM HEPES, pH 7.4.

Imaging

PLS was measured in populations of intact HEK293 cells grown on glass coverslips mounted in Attofluor chambers (Invitrogen) and imaged at ambient temperature with a Zeiss confocal microscope using a 63× Plan-Apochromat NA 1.4 objective. Binding of annexin V–Alexa Fluor 568 to patch-clamped cells during voltage-clamp recording was imaged with a wide-field Zeiss Axiovert 100 microscope using a 40× NA 0.6 LD-Acroplan objective. Images were acquired with an Orca-FLASH 4.0 digital CMOS camera (C11440; Hamamatsu) controlled by Metamorph 7.8 software (Molecular Devices). Images were analyzed using Fiji ImageJ 1.49.

RNA expression analysis

For real-time PCR, total RNA was collected from MPCs using PureLink RNA kit following the manufacturer's instructions (Invitrogen). All RNA samples were treated with DNase I (Invitrogen) according to the manufacturer's protocol to ensure purity. cDNA was generated from total RNA via reverse transcription reaction using SuperScript III reverse transcription (Invitrogen) and random hexamer primers. cDNA was then amplified using the SYBR Select Master Mix reagent (Applied Biosystems) and 2.5 µM of each primer. Real-time PCR reactions were performed and analyzed with StepOnePlus Real Time PCR System (Applied Biosystems), using GAPDH as an internal control. Fold-change of

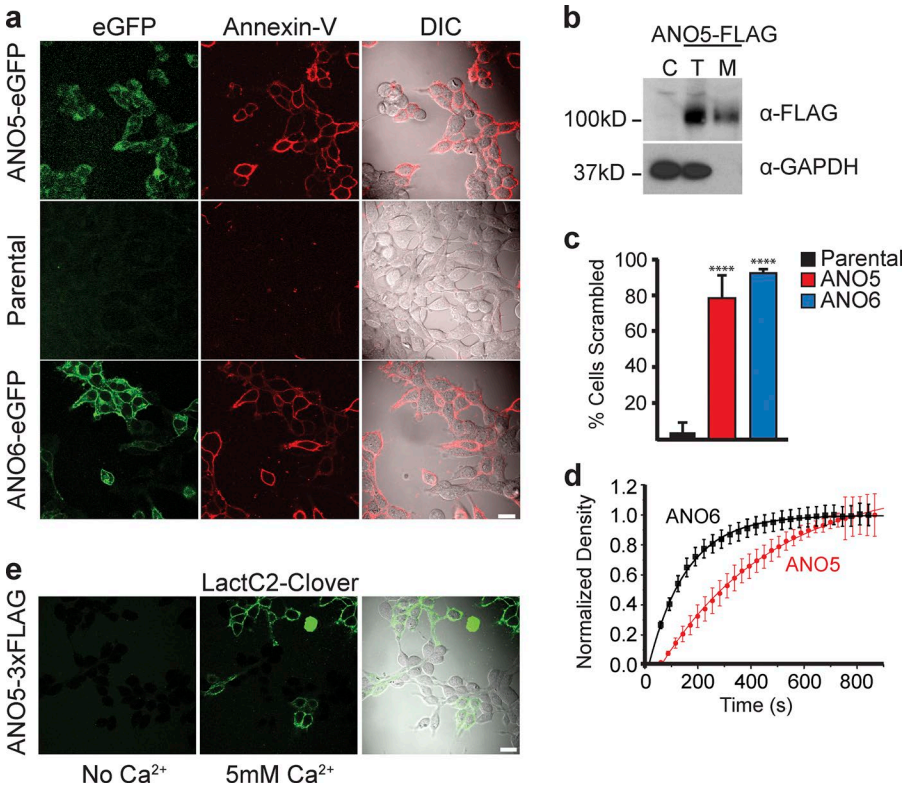

Figure 1. **ANO5 expression activates Ca^{2+}-PLS. (a)** HEK293 cell lines stably expressing eGFP-tagged ANOs or the parental HEK293 cells were stimulated using the store-operated Ca^{2+} entry assay for 10 min, and PtdSer exposure was monitored via annexin V–Alexa Fluor 568 binding. DIC, differential interference contrast. Scale bar, 20 µm . **(b)** Western blot of HEK293 cells expressing ANO5-3×FLAG. Cells were surface biotinylated, and the biotinylated surface membrane fraction was isolated using streptavidin beads. C, control untransfected lysate; M, anti-FLAG isolated surface biotinylated fraction from ANO5-3×FLAG transfected lysate; T, total ANO5-3×FLAG transfected lysate. GAPDH was used as a loading control and to show no cytoplasmic proteins are biotinylated (lower blot). **(c)** Quantification of the fraction of cells expressing Clover-tagged ANOs that were bound by the PtdSer probe LactC2-Cherry when stimulated using the store-operated Ca^{2+} entry assay for 10 min. Three independent experiments totaling >250 cells per condition. Error bars indicate SEM. Significance was evaluated via one-way ANOVA with Dunnett correction (****, P = 0.0001). **(d)** Time course of annexin V–Alexa Fluor 568 binding to HEK293 cells expressing ANO5-eGFP or ANO6-eGFP. Images of the same field of 30–100 cells were acquired at ∼20-s intervals. Mean pixel intensity ± SEM of more than three independent experiments. Mean pixel intensity at the end of the recordings were normalized to 1. **(e)** Binding of the PtdSer probe LactC2-Clover to a polyclonal population of HEK293 cells transfected with ANO5-3×FLAG. In the first panel, HEK cells were incubated with A23187 in the absence of Ca^{2+} for 10 min. In the second panel, Ca^{2+} was added. Scale bar, 20 µm.

gene expression was determined using the ΔΔCt method (Livak and Schmittgen, 2001). Multiple independent experiments were performed and analyzed in duplicate. The following qPCR primers were used: synANO5, 5′-CATGGAGCACAACACCTCCT-3′ (forward), 5′-TTGAGTTCAGCCGCCAGTAG-3′ (reverse); mAno6, 5′-CTTATCAGGAAGTATTACGGC-3′(forward), 5′-AGATATCCA TAGAGGAAGCAG-3′ (reverse); mGapdh, 5′-GGGTCCCAGCTTAGG TTCAT-3′ (forward), 5′-TACGGCCAAATCCGTTCACA-3′ (reverse).

Lentivirus

Synthetic hANO5 was subcloned into a modified version of the lentiviral transfer plasmid LJM1 (19319; Addgene; Sancak et al., 2008) under control of the PGK promoter and flanked by a viral 2A site and eGFP to mark infected cells. The PAX2 (12260; Addgene) packaging plasmid and pMD2.G envelope plasmid (12259; Addgene) were cotransfected into HEK293T cells using Lipofectamine 3000 (Invitrogen; manufacturer's protocol) along with *ANO5* transfer plasmid or scrambled transfer plasmid (1864; Addgene; Sarbassov et al., 2005), and viral supernates were collected at 24, 48, and 72 h after transfection. Viral supernates were filtered (0.45 µm), and lentiviral particles were concentrated using ultracentrifugation. Viral concentrations were estimated by ELISA for p24 to control for consistent infections between experiments and to calculate infectious units (IFUs; 632200; Takara Bio). MPCs were infected at low passage overnight in the presence of 8 µg/ml polybrene in growth media using indicated IFUs.

Results

ANO5 elicits PLS

ANO5 is very closely related to ANO6, with 48% identity in amino acid sequence (Whitlock and Hartzell, 2016). Because ANO6 elicits Ca^{2+}-PLS (Suzuki et al., 2010; Yu et al., 2015), we hypothesized that ANO5 is a PLSase and that perturbations in this activity are associated with changes in skeletal muscle function that contribute to the progression of LGMD2L. To test whether ANO5 is a PLSase, we measured the ability of ANO5 overexpression to confer Ca^{2+}-PLS in HEK-293 cells. We employed HEK293 cells as a model because they (1) do not natively express ANO5; (2) exhibit low endogenous Ca^{2+}-PLS activity, as described previously (Yu et al., 2015); and (3) are a good model for measuring ion channel conductances associated with Ca^{2+}-PLS.

Previous studies have suggested that ANO5 is located in intracellular organelles (Mizuta et al., 2007; Duran et al., 2012) and does not mediate PM scrambling (Suzuki et al., 2013). To confirm that ANO5 is present on the cell surface, surface proteins on HEK293 cells transfected with ANO5-3×FLAG were biotinylated using membrane-impermeant Sulfo-NHS-LC-biotin. Bi-

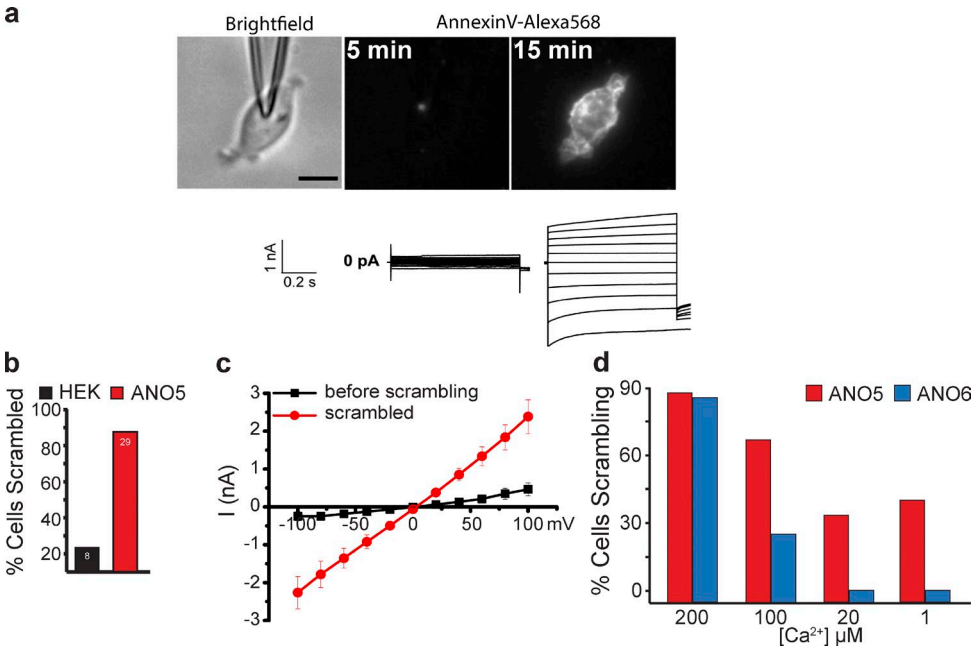

Figure 2. **ANO5-dependent Ca^{2+}-PLS is associated with an ionic current. (a)** Simultaneous measurement of annexin V–Alexa Fluor 568 binding and whole-cell patch clamp recording of ANO5-Clover HEK293 cells. Cells were patch-clamped with 200 µM free Ca^{2+} in the intracellular (pipette) solution, and currents were measured from a holding potential of 0 mV by voltage steps between −100 mV and +100 mV in 20-mV increments. Representative images (top) and corresponding currents (bottom) show a typical experiment of 29. The first panel is a bright-field image of the cell, and the second two images show fluorescence of bound annexin V. Scale bar, 10 µm. **(b)** Number of cells scrambled during patch-clamp experiments. White numbers indicate the number of cells. **(c)** Mean I–V relationships before (black squares) and after (red circles) cells showed significant annexin V binding. **(d)** Quantification of the percentage of cells bound by annexin V–Alexa Fluor 568 in ANO5-Clover or ANO6-Clover–expressing HEK293 cells when stimulated via whole-cell patch clamp as in panel a but with different concentrations of free Ca^{2+} in the intracellular (pipette) solution. Each condition represents data from >10 cells.

otinylated surface proteins were captured on streptavidin beads, run on SDS-PAGE gels, and Western blots probed with anti-FLAG antibody (Fig. 1 b). We found that a small fraction of ANO5 trafficked to the PM. Although ANO5 trafficking in HEK293 cells may not be representative of ANO5 trafficking in muscle, it provides a system to investigate the function of ANO5.

PtdSer exposure was monitored by binding of annexin V–Alexa Fluor 568 in response to elevation of intracellular Ca^{2+} by ionophore-stimulated store-operated Ca^{2+} entry (see Materials and methods; Fig. 1 a). Ca^{2+} stimulation elicited PtdSer exposure in the vast majority of cells expressing exogenous ANO5 in contrast to parental HEK293 cells, which do not exhibit this activity (Fig. 1 a). ANO5-mediated PLS developed at a rate slightly slower than that produced by ANO6, but both elicited maximal PtdSer exposure in ∼10 min (Fig. 1 d). We confirmed that the observed PtdSer exposure was Ca^{2+} dependent by using the PtdSer probe LactC2-Clover, which, unlike annexin V, does not require exogenous Ca^{2+} as a cofactor for binding. Treating transiently transfected ANO5-3×FLAG cells with ionophore in the absence of extracellular Ca^{2+} did not expose PtdSer as measured by LactC2-Clover binding (Fig. 1 e), but subsequent addition of Ca^{2+} rapidly exposed PtdSer. Thus, ANO5-dependent PtdSer exposure requires Ca^{2+}.

ANO5 PLS is associated with nonselective ionic currents

We have previously shown that ANO6 generates ionic currents that develop in parallel with PLS (Yu et al., 2015) and have suggested that this current represents ions that are conducted through the same pathway that conducts lipids (Whitlock and Hartzell, 2016, 2017; Jiang et al., 2017). To determine whether ANO5 also generates ionic currents, we performed whole-cell patch clamp of ANO5-expressing HEK293 cells while simultaneously measuring PLS by annexin V–Alexa Fluor 568 binding. Pipette (intracellular) solutions containing 200 µM free Ca^{2+} were used to activate ANO5. This high Ca^{2+} concentration was used because ANO6 has a low sensitivity to Ca^{2+} (Yu et al., 2015; Fig. 2 d). Both PLS and ionic currents developed slowly after elevation of cytosolic Ca^{2+} (Fig. 2 a). In general, both current and annexin V binding began to increase several minutes after establishing whole-cell recording and reached a plateau within 15 min. This is very similar to our previous observations of ANO6 (Yu et al., 2015). Under these patch-clamp conditions, ∼90% of ANO5-expressing cells scramble, while 25% of untransfected cells scramble (Fig. 2 b). Currents generally exhibited linear I–V relationships (Fig. 2 c) with slow activation at positive voltages and some deactivation at very negative voltages.

Ionic selectivity of ANO5 currents was determined by changing extracellular salt concentration, measuring the shift in reversal potential, and calculating the relative ionic permeabilities with the Goldmann–Hodgkin–Katz equation (Barry, 2006). A switch from symmetrical CsCl solutions on both sides of the membrane to a 10-fold lower concentration of extracellular CsCl results in only a modest ∼10-mV negative shift in the current's reversal potential (Fig. 3 a). This corresponds to a P_{Cs}/P_{Cl} permeability ratio of 1.6 (Fig. 3 b). A similar value was found for P_{Na}/P_{Cl} (Fig. 3 b). These data suggest that the ANO5 pore is weakly cation

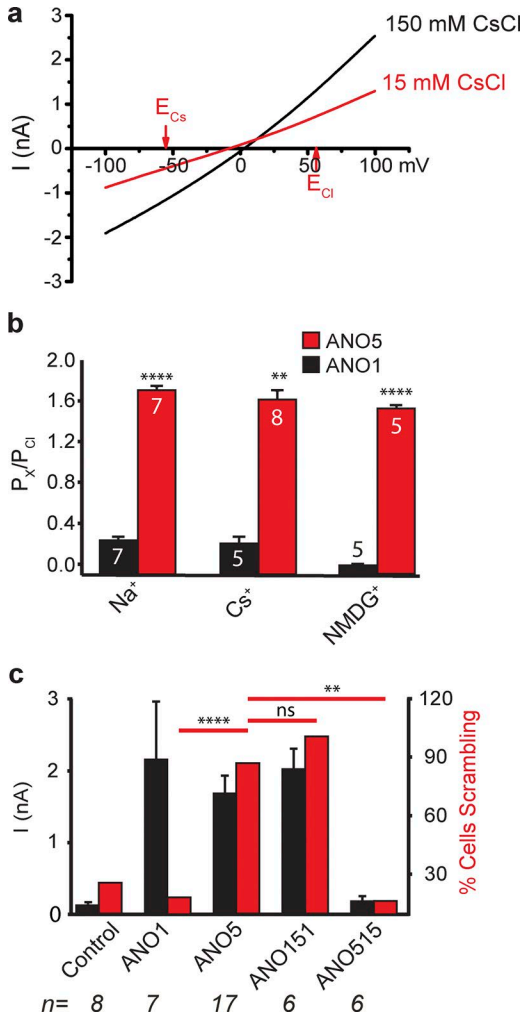

Figure 3. **ANO5-PLS associated ionic currents are nonselective. (a)** Representative whole-cell I–V curves recorded from ANO5-expressing HEK293 cells with 200 µM free Ca^{2+} in the pipette with external solutions containing 150 mM (black) or 15 mM (red) CsCl. Currents were generated by ramps from −100 to +100 mV. **(b)** Cation permeability of ANO5 and ANO1 currents relative to Cl^- (P_x/P_{Cl}) were calculated by changes in reversal potential as shown in panel a. Numbers in or above column indicate the number of cells assayed. Differences between ANO1 and ANO5 were evaluated for each condition using a paired Student's *t* test (**, P = 0.0012; ****, P = 0.0001). Differences in cation permeability for ANO5 were compared using a one-way ANOVA (P = 0.2693). **(c)** Ionic current amplitudes (black) and PLS (red) of HEK293 cells expressing ANO1, ANO5, and ANO1 harboring the ANO5 SCRD (ANO151) and ANO5 harboring the ANO1 SCRD ANO515. Differences in cells scrambling versus not scrambling were compared using a Fisher exact test (**, P = 0.0021; ****, P < 0.0001; ns, P = 0.5658). Numbers below indicate the number of cells assayed. Error bars indicate SEM.

selective. Further, the pore appears to be relatively large, because it is also permeable to the large organic cation $NMDG^+$, which has a mean diameter of >7 Å. These results are in sharp contrast to ANO1, which is highly Cl^- selective (Fig. 3 b).

To verify that the currents and PLS were mediated by ANO5 and not caused by up-regulation of another endogenous scramblase, we mutated the scramblase domain of ANO5. We previously identified a 34-amino-acid sequence that we call the scrambling domain (SCRD) in ANO6 that is necessary for Ca^{2+}-PLS (Yu et al., 2015). This sequence is highly conserved in ANO5. When the SCRD domain of ANO5 was replaced with the homologous domain from ANO1 ("ANO515"), PLS and the development of nonselective, scrambling-associated currents were greatly reduced (Fig. 3 c). In contrast, when the ANO5 SCRD was swapped into ANO1 ("ANO151"), it gave ANO1 the ability to scramble lipids and was associated with the development of nonselective, scrambling-associated currents. These results confirm that scrambling in ANO5-transfected HEK293 cells is dependent on ANO5.

MPC fusion and PtdSer exposure is defective in Ano5$^{-/-}$ MPCs

Having shown that ANO5 overexpression confers both PLS and ion currents to HEK293 cells, we then asked whether the loss of ANO5 in MPCs is associated with loss of Ca^{2+}-PLS and associated ionic currents. Previously, we characterized an *Ano5*$^{-/-}$ mouse model (Griffin et al., 2016) that was created by inserting a "gene trap" exogenous splice acceptor site followed by a premature stop codon between exons 8 and 9 (Fig. 4 a). A similar premature termination of *ANO5* is associated with most LGMD2L patients (c.191dupA) and is considered a LGMD2L founder mutation (Hicks et al., 2011). This mouse model recapitulates many aspects of LGMD2L and demonstrates defective cell–cell fusion of isolated MPCs (Griffin et al., 2016). This model exhibits a loss of ANO5 protein in two tissues (skeletal muscle and testis) that typically express high steady-state levels of ANO5 (Fig. 4 b).

MPCs were isolated from the hindlimbs of adult animals and patch-clamped with an internal (pipette) solution containing 200 µM free Ca^{2+} (Fig. 5 a). Ionic currents were measured by voltage steps, and PtdSer exposure was simultaneously measured by annexin V–Alexa Fluor 568 binding. A majority (>90%) of differentiated wild-type *Ano5*$^{+/+}$ MPCs expose PtdSer on the external surface and develop ionic currents characteristic of ANO5 currents after elevating cytosolic Ca^{2+} by establishing whole-cell recording with Ca^{2+} in the patch pipette (Fig. 5, a and b). Current amplitude and annexin V–Alexa Fluor 568 binding increased in parallel. The currents had biophysical properties similar to currents in ANO5-transfected HEK293 cells (Fig. 1): they had linear

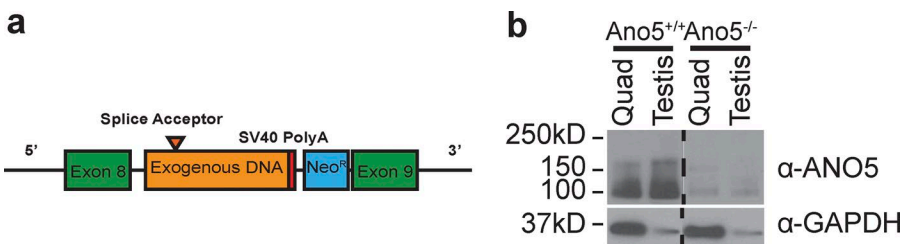

Figure 4. **Exogenous "gene trap" knock-in results in loss of ANO5. (a)** *Ano5* knockout construct. Briefly, a "gene trapping" element was inserted between exons 8 and 9 consisting of an exogenous splice acceptor followed by stop codons (Griffin et al., 2016). **(b)** Western blot of SDS-PAGE gel from lysates of quadriceps (Quad) or testis from 3-mo-old wild-type or *Ano5* knockout mice.

I–V relationships and exhibited slow activation at positive voltages and some deactivation at very negative voltages. In contrast, the majority of *Ano5*$^{-/-}$ cells (~75%) did not expose PtdSer when patch clamped with Ca^{2+} in the patch pipette and did not develop PLS-associated ionic currents (Fig. 5, a and b).

ANO5 is not the only scramblase expressed in MPCs. Most notably, MPCs also express significant levels of ANO6. We wondered whether the absence of PLS in *Ano5*$^{-/-}$ MPCs might be explained by down-regulation of ANO6 in addition to loss of ANO5 expression. However, Western blot showed that ANO6 levels were comparable in differentiated *Ano5*$^{+/+}$ and *Ano5*$^{-/-}$ MPCs (Fig. 5 c). This result demonstrates that the absence of scrambling in *Ano5*$^{-/-}$ cells is not explained by changes in ANO6 steady-state levels. However, it raises the question why the ANO6 that is present does not mediate scrambling in the *Ano5*$^{-/-}$ cells (see Discussion).

MPC PLS and fusion are rescued by infection with ANO5 virus

If ANO5 elicits Ca^{2+}-PLS and plays an important role in MPC fusion, then it should be possible to rescue the defective fusion of *Ano5*$^{-/-}$ MPCs by overexpressing human *ANO5*. Furthermore, this rescued fusion should be accompanied by rescued Ca^{2+}-PLS and ionic currents. We chose culture conditions that generated robust myotube development following ~36 h of *Ano5*$^{+/+}$ MPC differentiation (Fig. 6 a). The ability of cells to form multinucleated myotubes was measured by counting the number of nuclei (DAPI stained) per myotube (phalloidin stained) in *Ano5*$^{+/+}$, *Ano5*$^{-/-}$, and *Ano5*$^{-/-}$ MPCs treated with lentivirus expressing a scrambled sequence or *Ano5*$^{-/-}$ MPCs treated with lentivirus expressing a synthetic, codon-optimized *hANO5* under control of the phosphoglycerate kinase promotor (Fig. 6 b). Previous investigations have demonstrated that lentivirus is robust in introducing stably integrated transgenes in MPCs (Li et al., 2005). Additionally, unlike promotors that are readily silenced via methylation in muscle (e.g., cytomegalovirus), the phosphoglycerate kinase promotor produces reliable, consistent expression of virally introduced transgenes in muscle cells (Brooks et al., 2004; Jackson et al., 2013). The images (Fig. 6 a), cumulative frequency plot (Fig. 6 e), and frequency histogram (Fig. 6 f) show that *Ano5*$^{+/+}$ MPCs formed myotubes having more nuclei compared with *Ano5*$^{-/-}$ MPCs. Most importantly, expression of *hANO5* in the *Ano5*$^{-/-}$ MPCs significantly rescued the fusion defect. For example, only ~25% of the nuclei in wild-type MPCs were found in myotubes having less than five nuclei, but loss of *Ano5* resulted in ~50% of the nuclei in myotubes with less than five nuclei (Fig. 6 d). Infection with *hANO5* lentivirus significantly reduces the percentage of nuclei in myotubes with less than five nuclei from 50% to 26% (v1.3 infectious units [IFUs]) or 30% (v13 IFUs), very close to the wild-type value. The lentiviral introduction of *hANO5* did not change the steady-state level of *Ano6* transcript, so the effects of *hANO5* rescue are not the result of simply up-regulating *Ano6* (Fig. 6 c).

The rescue of fusion by expression of *hANO5* was accompanied by the rescue of Ca^{2+}-PLS in *Ano5*$^{-/-}$ MPCs. Although only ~25% of *Ano5*$^{-/-}$ MPCs expose PtdSer when stimulated with 200 µM free intracellular Ca^{2+}, >80% expose PtdSer following *hANO5* rescue (Fig. 7, a and b). Moreover, *hANO5*-rescued PLS is accompanied by a nonselective ionic current (Fig. 7 c). These

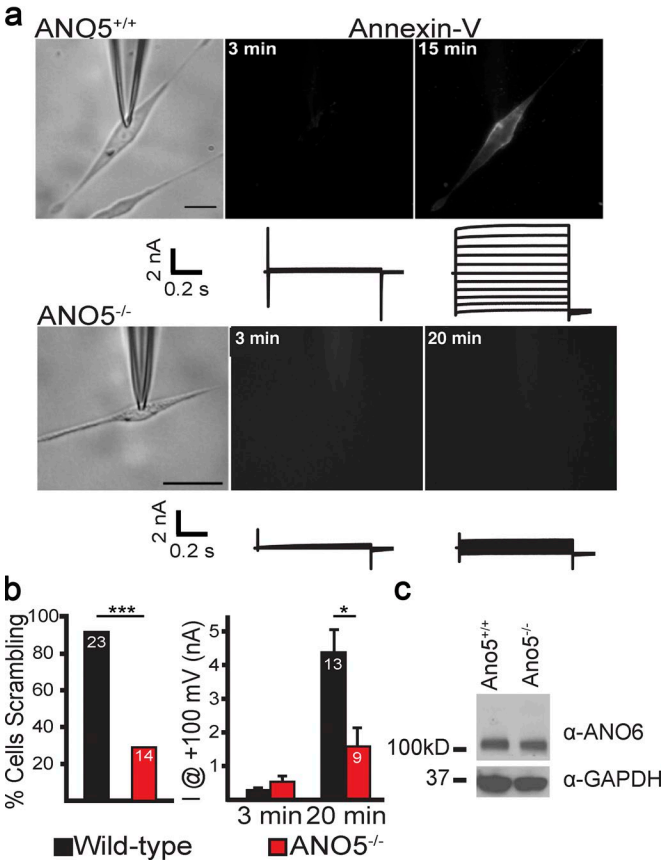

Figure 5. ***Ano5*$^{-/-}$ muscle cells exhibit perturbed Ca^{2+}-PLS and PLS-associated ionic current. (a)** Simultaneous whole-cell patch clamp and annexin V–Alexa Fluor 568 binding of primary MPCs differentiated for ~24 hr. Images on the left show bright-field micrographs of patch-clamped MPCs. Center and right images show annexin V–Alexa Fluor 568 binding. Scale bars, 10 µm. Below the images are ionic currents recorded using voltage steps between +100 and −100 mV in 20-mV increments from a holding potential of 0 mV. **(b)** Quantification of Ca^{2+}-PLS in MPCs (left), and average current of differentiated myoblasts at +100 mV (right). The statistical difference in Ca^{2+}-PLS between genotypes was calculated using a Fisher exact test (***, P = 0.0001). The current at 20 min was statistically evaluated using a paired Student's *t* test (*, P = 0.026). The white numbers in the columns indicate the number of cells assayed. The same cells were measured at 3 and 20 min. Error bars indicate SEM. **(c)** Western blot of native ANO6 levels in wild-type and *Ano5* knockout MPCs differentiated for ~24 h.

Ca^{2+}-stimulated currents were significantly larger when compared with currents in *Ano5*$^{-/-}$ MPCs (P = 0.027; Fig. 7 d). Similar to ANO5-dependent currents in wild-type MPCs, ANO5 rescued currents exhibited a linear I–V relationship (Fig. 7 e).

Discussion

ANO5 is probably a PLSase

Here, we demonstrate that like ANO6, heterologous overexpression of ANO5 in HEK293 cells elicits Ca^{2+}-PLS (Suzuki et al., 2010, 2013; Yu et al., 2015). Mutations in the ANO5 SCRD destroy its scrambling activity, while this same region confers Ca^{2+}-PLS to the calcium-activated chloride channel ANO1. Moreover, MPCs isolated from mice lacking Ano5 exhibit a significant loss of Ca^{2+}-PLS that can be rescued with the introduction of exogenous

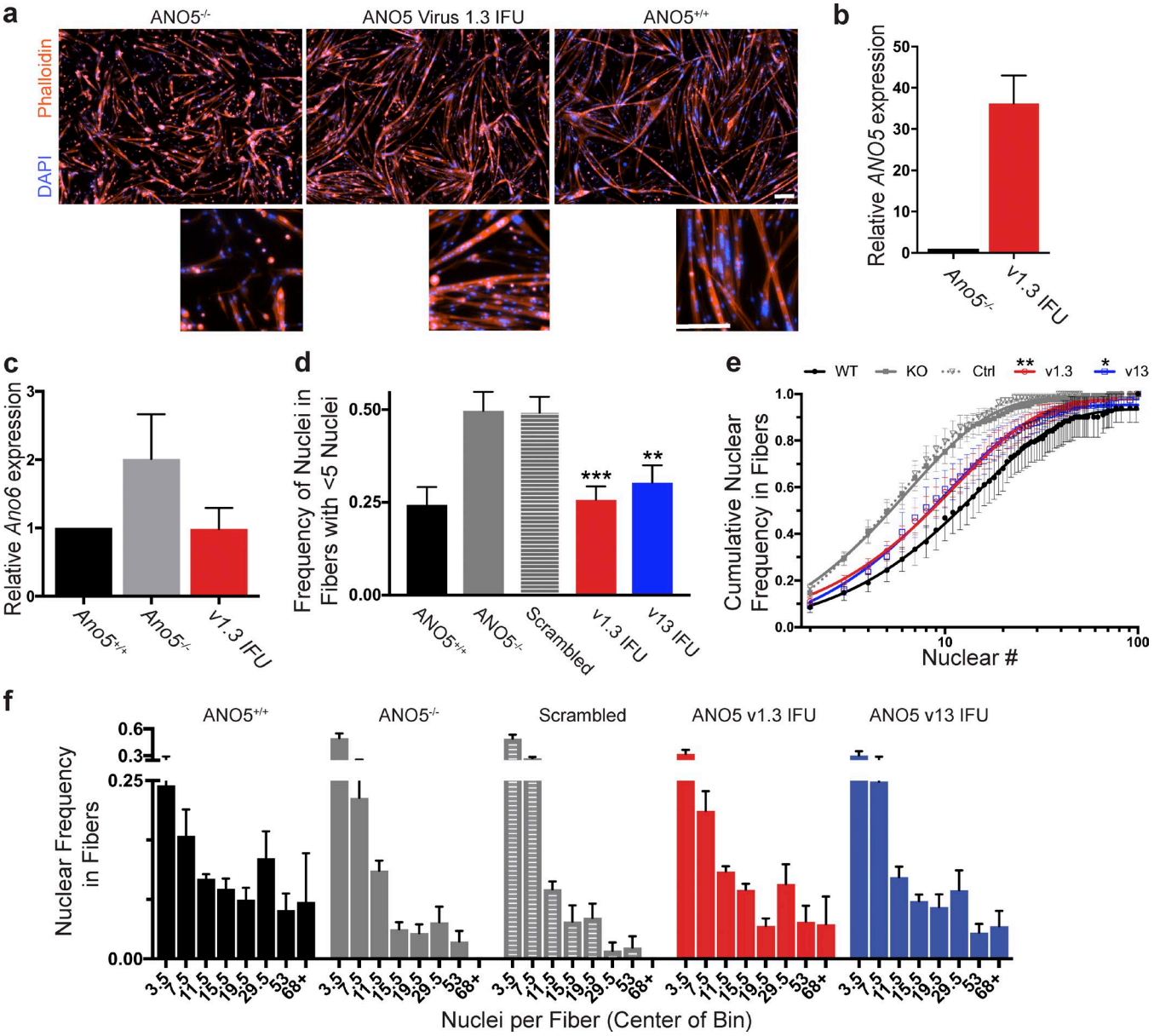

Figure 6. **Exogenous ANO5 expression rescues Ano5$^{-/-}$ MPC fusion. (a)** Representative images of MPC fusion after ∼36 h differentiation for *Ano5*$^{+/+}$, *Ano5*$^{-/-}$, and *Ano5*$^{-/-}$ cells rescued with 1.3 IFUs of ANO5 virus. Scale bars, 300 µm. **(b)** Quantitative PCR evaluation of steady-state *ANO5* transcript levels, following viral infection, normalized to *Gapdh*. Error bars indicate SEM. **(c)** Quantitative PCR evaluation of steady-state, endogenous *Ano6* levels normalized to *Gapdh*. **(d)** Frequency of nuclei in fibers containing less than five nuclei. Ano5$^{+/+}$ represents three independent experiments with three independently isolated cell lines (>6,500 nuclei). *Ano5*$^{-/-}$, *ANO5* 1.3 IFU, and ANO5 13 IFU represent five independent experiments, with three independently isolated cell lines (>7,000 nuclei per condition). Error bars represent SEM. Significance was determined by one-way ANOVA with Dunnett correction (***, P = 0.0003; **, P = 0.0013). **(e)** Cumulative frequency of nuclei per fiber size. Nuclei per fiber distributions were evaluated by fitting the data for each replicate in each condition to a single exponential. The exponential constants for each condition were statistically compared to *Ano5*$^{-/-}$ using a one-way ANOVA with Dunnett correction (**, P = 0.0095 and *, P = 0.04). **(f)** Raw frequency histogram representation of data. The values on thex axis represent the center of the bins for number of nuclei per fiber. Error bars represent SEM.

ANO5. Although these results strongly suggest that ANO5 is a PLSase, this conclusion will remain tentative until the protein has been purified and reconstituted. A previous report suggested that transient transfection of cells with *Ano5* did not support PLS (Suzuki et al., 2013). These results may differ from our findings for a number of reasons. While Suzuki et al. (2013) used a transiently transfected thymocyte cell model that expressed murine ANO5 at very low levels, we evaluated the Ca^{2+}-PLS competence of a codon-optimized human *ANO5* in a stably transfected human cell line and confirmed that ANO5 partially trafficked to the PM (see Materials and methods).

As has previously been described for other ANO scramblases (nhTMEM16, afTMEM16, and ANO6; Suzuki et al., 2010; Malvezzi et al., 2013; Brunner et al., 2014; Yu et al., 2015; Jiang et al., 2017), ANO5-dependent Ca^{2+}-PLS is tightly associated with the simultaneous development of nonselective or weakly cation-selective

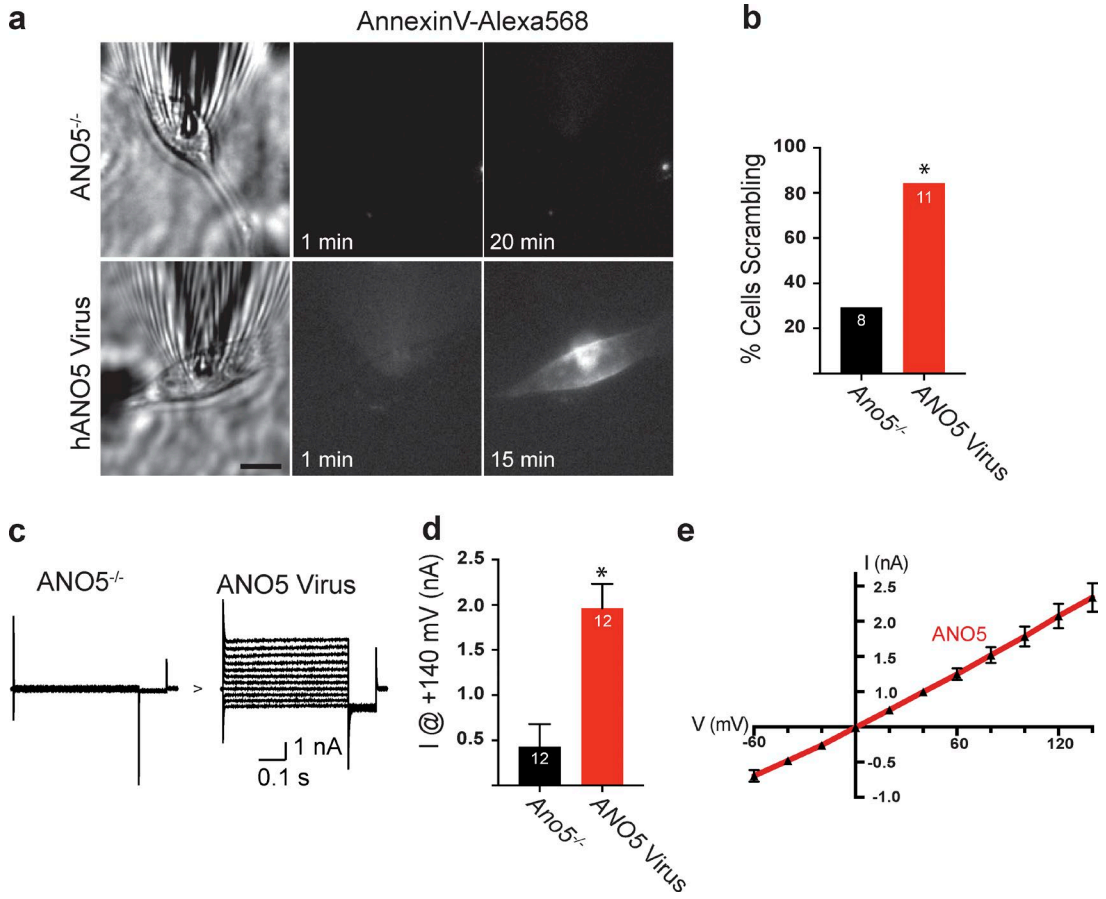

Figure 7. **Exogenous ANO5 expression rescues Ano5$^{-/-}$ MPC Ca^{2+}-PLS. (a)** Simultaneous whole-cell patch clamp and annexin V–Alexa Fluor 568 binding as an indicator of Ca^{2+}-PLS of primary MPCs differentiated for ∼24 h. Images on the left show bright-field micrographs of patched MPCs. Images at the center and right show annexin V binding. Scale bar, 10 µm. **(b)** Quantification of Ca^{2+}-PLS in MPCs. Statistical significance was measured using a Fisher exact test (*, P = 0.024). **(c)** Representative traces of ionic currents from MPCs isolated from the same mouse with or without ANO5 virus rescue following 10 min of whole-cell patch clamp with 200 µM Ca^{2+} intracellular solution. > denotes 0 nA. 20mV voltage steps from −60 mV to 140 mV. **(d)** Quantification of ionic currents from cell lines isolated from two 3-mo-old mice with and without viral rescue (*, P = 0.027, paired *t* test). **(e)** Current–voltage relationship *ANO5* rescued *Ano5*$^{-/-}$ MPCs from panel d.

ionic currents that we believe may be a consequence of membrane disturbances created by lipid translocation.

Loss of ANO5 is associated with defective MPC fusion

The loss of ANO5-dependent Ca^{2+}-PLS and PLS-associated ionic currents is associated with a significant decrease in the ability of MPCs to produce myotubes having many nuclei. Although fusion is clearly perturbed, it is not abolished in the ANO5$^{-/-}$ cells. This suggests the possibility that the initial fusion events are not impaired, but the accretion of subsequent fusion events is decreased. In *Drosophila melanogaster*, myotube formation occurs in two steps. The primary fusion events occur between two different types of mononucleated cells: founder cells and fusion-competent myoblasts. The myotubes then increase in mass and nuclear number by secondary fusion events that use slightly different machinery (Kim et al., 2015). It is not clear whether vertebrates also use different mechanisms for early and late fusion, but we propose that ANO5 regulates or coordinates fusion steps that lead to the accumulation of large numbers of nuclei in the muscle fibers.

The perturbation in fusion could occur at one of several steps, including proliferation and differentiation of fusion-competent cells, migration of cells to the site of fusion, recognition and adhesion of fusion-competent cells, and formation of the fusion pore between cells (Chen and Olson, 2004; Abmayr and Pavlath, 2012). While we cannot distinguish between the role of ionic currents and PLS in the MPC fusion process because the two activities are tightly linked, we prefer the hypothesis that PLS is a key event because PtdSer apparently plays an integral role (van den Eijnde et al., 1997, 2001) in myoblast fusion. Prolonged exposure (5 d) to the PtdSer-binding protein, annexin V, or PtdSer antibody during myoblast fusion significantly inhibits the formation of myotubes. Additionally, liposomes of PtdSer, but not phosphatidylcholine, stimulate myoblast fusion (van den Eijnde et al., 2001; Jeong and Conboy, 2011). Moreover, it has recently been reported that the PtdSer receptors BAI1 and STAB2 participate in myoblast fusion (Hochreiter-Hufford et al., 2013; Park et al., 2016). Because PLS is known to alter the biophysical properties of cell membranes such as curvature and electrostatics (Whitlock and Hartzell, 2017), it is tempting to propose that PLS may play a role in overcoming the energy barriers for leaflets of fusing membranes to merge together. ANO5 ionic currents could also be important in regulating myoblast fusion by regulating membrane potential or in-

tracellular Ca^{2+} concentration. Another possibility is that PLS is secondary or parallel to the primary event.

These data provide additional insights into our previous observation that the ability of muscle to regenerate in vivo in response to cardiotoxin injury is greatly diminished in this *Ano5*$^{-/-}$ knockout model (Griffin et al., 2016). Although it is possible that ANO5 has other functions within the cell, the fact that the loss of ANO5-dependent Ca^{2+}-PLS and associated currents is correlated with diminished MPC fusion competence strongly suggests that these functions of ANO5 contribute to the perturbed muscle repair and ANO5 myopathy phenotype observed in our model. Although we have focused on the role of ANO5 in coordinating MPC fusion, it is possible that ANO5 also facilitates muscle repair in other ways. In particular, repair of isolated muscle fibers after laser damage, a process that does not rely on progenitor cell fusion (Cooper and Head, 2015), is diminished in the *Ano5*$^{-/-}$ mouse (Griffin et al., 2016). Nevertheless, our observations here, our previous characterization of a LGMD2L-like phenotype in this model, and data from other investigators demonstrating PtdSer exposure in MPC fusion (van den Eijnde et al., 1997, 2001; Hochreiter-Hufford et al., 2013; Park et al., 2016) support the hypothesis that the loss of ANO5-dependent Ca^{2+}-PLS likely contributes to the development and/or progression of LGMD2L by perturbing MPC fusion coordination.

Subcellular location of ANO5 and its role in scrambling

ANO5 seems to be located largely in intracellular membranes, both in muscle (Mizuta et al., 2007; Xu et al., 2018) and in transfected HEK293 cells (our data). If so, how does it mediate PLS on the PM? One possibility is that the small amount of ANO5 on the PM is sufficient. Another possibility is that PM scrambling is a consequence of membrane or lipid trafficking from intracellular membranes. There have been suggestions in the literature that scrambling involves membrane trafficking (Mirnikjoo et al., 2009; Lee et al., 2013). Furthermore, ANO-dependent Ca^{2+}-PLS is associated with the release of extracellular vesicles (Sims et al., 1989; Comfurius et al., 1990; Fujii et al., 2015). This raises the possibility that ANO5 influences muscle cell repair through mechanisms that are not localized exclusively at the PM. In this regard, both exocytosis and endocytosis have been implicated to be important in myoblast fusion (Kim et al., 2015), and it has been suggested that extracellular vesicles may play a role in muscle development and regeneration (Demonbreun and McNally, 2017; Guescini et al., 2017), although this remains unproven.

Why is Ca^{2+}-PLS defective in Ano5$^{-/-}$ MPCs despite ANO6 expression?

It has been suggested that ANOs 3, 4, 5, 6, 7, and 9 are PLSases (Suzuki et al., 2013). Certainly, there is good evidence that different ANOs are expressed in a tissue-specific manner, but most tissues express multiple ANO scramblases (Suzuki et al., 2013). Muscle expresses both ANO5 and ANO6 (in addition to ANO8 and ANO10), but surprisingly *Ano5*$^{-/-}$ MPCs exhibit defective Ca^{2+}-PLS despite the presence of ANO6. These data suggest that despite their similar functions, ANO5 and ANO6 play different roles and/or are regulated differently in muscle cells. Another possibility is that ANO5 is not itself a scramblase, but a scramblase regulator, possibly forming a complex with ANO6. However, knockdown or rescue of *Ano5* does not seem to have major effects on *Ano6* expression or endogenous ANO6 steady-state levels. Thus, changes in Ca^{2+}-PLS do not stem from altered levels of ANO6. Our mutagenesis shows that ANO5 is required to elicit Ca^{2+}-PLS, and that this activity does not stem from exogenous ANO5 up-regulating an endogenous scramblase like ANO6.

It is important to note that two other laboratories have reported *Ano5*$^{-/-}$ mouse models that have no muscle phenotype (Gyobu et al., 2015; Xu et al., 2015). Recently, one of these laboratories has also produced a rabbit *Ano5*$^{-/-}$ model by disrupting *Ano5* at exons 12 and 13, similar to our murine model, and this model exhibits dystrophic phenotypes similar to our murine model (Sui et al., 2018). We are unable to explain why our mouse has a noticeable-yet mild-skeletal muscle phenotype while other murine models do not. These discrepancies may be the result of genetic differences in the murine models, the different approaches to disrupt *Ano5*, or other factors. However, the ability of our *ANO5* lentivirus to rescue Ca^{2+}-PLS, PLS-associated ion currents, and fusion coordination in *Ano5*$^{-/-}$ MPCs suggests that the defects we describe here result from the loss of ANO5.

Acknowledgments

The LactC2 probe was a gift from L. Chernomordik (National Institute of Child Health and Development, Bethesda, MD) (Zaitseva et al., 2017). pLJM1-EGFP (Addgene plasmid 19319) and scrambled plasmid (Addgene plasmid 1864) were gifts from D. Sabatini (Massachusetts Institute of Technology, Boston, MA). pMD2.G (Addgene plasmid 12259) and psPAX2 (Addgene plasmid 12260) were gifts from D. Trono (École polytechnique fédérale de Lausanne, Lausanne, Switzerland). The mouse model was a gift from the Jain Foundation and L. Rodino-Klapac (Nationwide Children's Hospital, Columbus, OH; Griffin et al., 2016).

This work was supported by the National Institutes of Health (grants AR067786 and EY114852) and the Muscular Dystrophy Association (grant MDA347440 to H.C. Hartzell). J. Whitlock was supported by a Ruth L. Kirschstein National Research Service Award (F31 GM116556-01A1).

The authors declare no competing financial interests.

Author contributions: J.M. Whitlock and H.C. Hartzell conceived the research and wrote the manuscript. J.M. Whitlock, H.C. Hartzell, and K. Yu designed and performed experiments and analyzed data. Y.Y. Cui managed the mouse colony and designed and created plasmids .

Eduardo Ríos served as editor.

Submitted: 17 April 2018
Revised: 12 August 2018
Accepted: 10 September 2018

References

Abmayr, S.M., and G.K. Pavlath. 2012. Myoblast fusion: lessons from flies and mice. *Development.* 139:641–656. https://doi.org/10.1242/dev.068353

Bansal, D., and K.P. Campbell. 2004. Dysferlin and the plasma membrane repair in muscular dystrophy. *Trends Cell Biol.* 14:206–213. https://doi.org/10.1016/j.tcb.2004.03.001

Barry, P.H. 2006. The reliability of relative anion-cation permeabilities deduced from reversal (dilution) potential measurements in ion channel studies. *Cell Biochem. Biophys.* 46:143–154. https://doi.org/10.1385/CBB:46:2:143

Bethel, N.P., and M. Grabe. 2016. Atomistic insight into lipid translocation by a TMEM16 scramblase. *Proc. Natl. Acad. Sci. USA.* 113:14049–14054. https://doi.org/10.1073/pnas.1607574113

Bevers, E.M., and P.L. Williamson. 2010. Phospholipid scramblase: an update. *FEBS Lett.* 584:2724–2730. https://doi.org/10.1016/j.febslet.2010.03.020

Bevers, E.M., and P.L. Williamson. 2016. Getting to the Outer Leaflet: Physiology of Phosphatidylserine Exposure at the Plasma Membrane. *Physiol. Rev.* 96:605–645. https://doi.org/10.1152/physrev.00020.2015

Bolduc, V., G. Marlow, K.M. Boycott, K. Saleki, H. Inoue, J. Kroon, M. Itakura, Y. Robitaille, L. Parent, F. Baas, et al. 2010. Recessive mutations in the putative calcium-activated chloride channel Anoctamin 5 cause proximal LGMD2L and distal MMD3 muscular dystrophies. *Am. J. Hum. Genet.* 86:213–221. https://doi.org/10.1016/j.ajhg.2009.12.013

Brooks, A.R., R.N. Harkins, P. Wang, H.S. Qian, P. Liu, and G.M. Rubanyi. 2004. Transcriptional silencing is associated with extensive methylation of the CMV promoter following adenoviral gene delivery to muscle. *J. Gene Med.* 6:395–404. https://doi.org/10.1002/jgm.516

Brunner, J.D., N.K. Lim, S. Schenck, A. Duerst, and R. Dutzler. 2014. X-ray structure of a calcium-activated TMEM16 lipid scramblase. *Nature.* 516:207–212. https://doi.org/10.1038/nature13984

Brunner, J.D., S. Schenck, and R. Dutzler. 2016. Structural basis for phospholipid scrambling in the TMEM16 family. *Curr. Opin. Struct. Biol.* 39:61–70. https://doi.org/10.1016/j.sbi.2016.05.020

Caputo, A., E. Caci, L. Ferrera, N. Pedemonte, C. Barsanti, E. Sondo, U. Pfeffer, R. Ravazzolo, O. Zegarra-Moran, and L.J. Galietta. 2008. TMEM16A, a membrane protein associated with calcium-dependent chloride channel activity. *Science.* 322:590–594. https://doi.org/10.1126/science.1163518

Chen, E.H., and E.N. Olson. 2004. Towards a molecular pathway for myoblast fusion in Drosophila. *Trends Cell Biol.* 14:452–460. https://doi.org/10.1016/j.tcb.2004.07.008

Collins, C.A., I. Olsen, P.S. Zammit, L. Heslop, A. Petrie, T.A. Partridge, and J.E. Morgan. 2005. Stem cell function, self-renewal, and behavioral heterogeneity of cells from the adult muscle satellite cell niche. *Cell.* 122:289–301. https://doi.org/10.1016/j.cell.2005.05.010

Comfurius, P., J.M. Senden, R.H. Tilly, A.J. Schroit, E.M. Bevers, and R.F. Zwaal. 1990. Loss of membrane phospholipid asymmetry in platelets and red cells may be associated with calcium-induced shedding of plasma membrane and inhibition of aminophospholipid translocase. *Biochim. Biophys. Acta.* 1026:153–160. https://doi.org/10.1016/0005-2736(90)90058-V

Cooper, S.T., and S.I. Head. 2015. Membrane Injury and Repair in the Muscular Dystrophies. *Neuroscientist.* 21:653–668. https://doi.org/10.1177/1073858414558336

Corrotte, M., P.E. Almeida, C. Tam, T. Castro-Gomes, M.C. Fernandes, B.A. Millis, M. Cortez, H. Miller, W. Song, T.K. Maugel, and N.W. Andrews. 2013. Caveolae internalization repairs wounded cells and muscle fibers. *eLife.* 2:e00926. https://doi.org/10.7554/eLife.00926

Demonbreun, A.R., and E.M. McNally. 2017. Muscle cell communication in development and repair. *Curr. Opin. Pharmacol.* 34:7–14. https://doi.org/10.1016/j.coph.2017.03.008

Di Zanni, E., A. Gradogna, J. Scholz-Starke, and A. Boccaccio. 2018. Gain of function of TMEM16E/ANO5 scrambling activity caused by a mutation associated with gnathodiaphyseal dysplasia. *Cell. Mol. Life Sci.* 75:1657–1670. https://doi.org/10.1007/s00018-017-2704-9

Dumont, N.A., C.F. Bentzinger, M.C. Sincennes, and M.A. Rudnicki. 2015. Satellite Cells and Skeletal Muscle Regeneration. *Compr. Physiol.* 5:1027–1059. https://doi.org/10.1002/cphy.c140068

Duran, C., Z. Qu, A.O. Osunkoya, Y. Cui, and H.C. Hartzell. 2012. ANOs 3-7 in the anoctamin/Tmem16 Cl- channel family are intracellular proteins. *Am. J. Physiol. Cell Physiol.* 302:C482–C493. https://doi.org/10.1152/ajpcell.00140.2011

Endo, T. 2015. Glycobiology of α-dystroglycan and muscular dystrophy. *J. Biochem.* 157:1–12. https://doi.org/10.1093/jb/mvu066

Fujii, T., A. Sakata, S. Nishimura, K. Eto, and S. Nagata. 2015. TMEM16F is required for phosphatidylserine exposure and microparticle release in activated mouse platelets. *Proc. Natl. Acad. Sci. USA.* 112:12800–12805. https://doi.org/10.1073/pnas.1516594112

Glover, L., and R.H. Brown Jr. 2007. Dysferlin in membrane trafficking and patch repair. *Traffic.* 8:785–794. https://doi.org/10.1111/j.1600-0854.2007.00573.x

Griffin, D.A., R.W. Johnson, J.M. Whitlock, E.R. Pozsgai, K.N. Heller, W.E. Grose, W.D. Arnold, Z. Sahenk, H.C. Hartzell, and L.R. Rodino-Klapac. 2016. Defective membrane fusion and repair in Anoctamin5-deficient muscular dystrophy. *Hum. Mol. Genet.* 25:1900–1911. https://doi.org/10.1093/hmg/ddw063

Guescini, M., S. Maggio, P. Ceccaroli, M. Battistelli, G. Annibalini, G. Piccoli, P. Sestili, and V. Stocchi. 2017. Extracellular Vesicles Released by Oxidatively Injured or Intact C2C12 Myotubes Promote Distinct Responses Converging toward Myogenesis. *Int. J. Mol. Sci.* 18:2488. https://doi.org/10.3390/ijms18112488

Gurevich, D.B., P.D. Nguyen, A.L. Siegel, O.V. Ehrlich, C. Sonntag, J.M. Phan, S. Berger, D. Ratnayake, L. Hersey, J. Berger, et al. 2016. Asymmetric division of clonal muscle stem cells coordinates muscle regeneration in vivo. *Science.* 353:aad9969. https://doi.org/10.1126/science.aad9969

Gyobu, S., H. Miyata, M. Ikawa, D. Yamazaki, H. Takeshima, J. Suzuki, and S. Nagata. 2015. A Role of TMEM16E Carrying a Scrambling Domain in Sperm Motility. *Mol. Cell. Biol.* 36:645–659. https://doi.org/10.1128/MCB.00919-15

Hamoud, N., V. Tran, L.P. Croteau, A. Kania, and J.F. Côté. 2014. G-protein coupled receptor BAI3 promotes myoblast fusion in vertebrates. *Proc. Natl. Acad. Sci. USA.* 111:3745–3750. https://doi.org/10.1073/pnas.1313886111

Han, R., and K.P. Campbell. 2007. Dysferlin and muscle membrane repair. *Curr. Opin. Cell Biol.* 19:409–416. https://doi.org/10.1016/j.ceb.2007.07.001

Hicks, D., A. Sarkozy, N. Muelas, K. Köehler, A. Huebner, G. Hudson, P.F. Chinnery, R. Barresi, M. Eagle, T. Polvikoski, et al. 2011. A founder mutation in Anoctamin 5 is a major cause of limb-girdle muscular dystrophy. *Brain.* 134:171–182. https://doi.org/10.1093/brain/awq294

Hochreiter-Hufford, A.E., C.S. Lee, J.M. Kinchen, J.D. Sokolowski, S. Arandjelovic, J.A. Call, A.L. Klibanov, Z. Yan, J.W. Mandell, and K.S. Ravichandran. 2013. Phosphatidylserine receptor BAI1 and apoptotic cells as new promoters of myoblast fusion. *Nature.* 497:263–267. https://doi.org/10.1038/nature12135

Jackson, M.F., K.E. Hoversten, J.M. Powers, G.D. Trobridge, and B.D. Rodgers. 2013. Genetic manipulation of myoblasts and a novel primary myosatellite cell culture system: comparing and optimizing approaches. *FEBS J.* 280:827–839.

Jaiswal, J.K., G. Marlow, G. Summerill, I. Mahjneh, S. Mueller, M. Hill, K. Miyake, H. Haase, L.V. Anderson, I. Richard, et al. 2007. Patients with a non-dysferlin Miyoshi myopathy have a novel membrane repair defect. *Traffic.* 8:77–88. https://doi.org/10.1111/j.1600-0854.2006.00505.x

Jeong, J., and I.M. Conboy. 2011. Phosphatidylserine directly and positively regulates fusion of myoblasts into myotubes. *Biochem. Biophys. Res. Commun.* 414:9–13. https://doi.org/10.1016/j.bbrc.2011.08.128

Jiang, T., K. Yu, H.C. Hartzell, and E. Tajkhorshid. 2017. Lipids and ions traverse the membrane by the same physical pathway in the nhTMEM16 scramblase. *eLife.* 6:e28671. https://doi.org/10.7554/eLife.28671

Kim, G.W., S.Y. Park, and I.S. Kim. 2016. Novel function of stabilin-2 in myoblast fusion: the recognition of extracellular phosphatidylserine as a "fuse-me" signal. *BMB Rep.* 49:303–304. https://doi.org/10.5483/BMBRep.2016.49.6.078

Kim, J.H., P. Jin, R. Duan, and E.H. Chen. 2015. Mechanisms of myoblast fusion during muscle development. *Curr. Opin. Genet. Dev.* 32:162–170. https://doi.org/10.1016/j.gde.2015.03.006

Lee, B.C., A.K. Menon, and A. Accardi. 2016. The nhTMEM16 Scramblase Is Also a Nonselective Ion Channel. *Biophys. J.* 111:1919–1924. https://doi.org/10.1016/j.bpj.2016.09.032

Lee, S.H., X.W. Meng, K.S. Flatten, D.A. Loegering, and S.H. Kaufmann. 2013. Phosphatidylserine exposure during apoptosis reflects bidirectional trafficking between plasma membrane and cytoplasm. *Cell Death Differ.* 20:64–76. https://doi.org/10.1038/cdd.2012.93

Li, S., E. Kimura, B.M. Fall, M. Reyes, J.C. Angello, R. Welikson, S.D. Hauschka, and J.S. Chamberlain. 2005. Stable transduction of myogenic cells with lentiviral vectors expressing a minidystrophin. *Gene Ther.* 12:1099–1108. https://doi.org/10.1038/sj.gt.3302505

Liewluck, T., and M. Milone. 2018. Untangling the complexity of limb-girdle muscular dystrophies. *Muscle Nerve.* 58:167–177. https://doi.org/10.1002/mus.26077

Livak, K.J., and T.D. Schmittgen. 2001. Analysis of relative gene expression data using real-time quantitative PCR and the 2(-Delta Delta C(T)) Method. *Methods.* 25:402–408. https://doi.org/10.1006/meth.2001.1262

Mahjneh, I., J. Jaiswal, A. Lamminen, M. Somer, G. Marlow, S. Kiuru-Enari, and R. Bashir. 2010. A new distal myopathy with mutation in anoctamin 5. *Neuromuscul. Disord.* 20:791–795. https://doi.org/10.1016/j.nmd.2010.07.270

Malvezzi, M., M. Chalat, R. Janjusevic, A. Picollo, H. Terashima, A.K. Menon, and A. Accardi. 2013. Ca2+-dependent phospholipid scrambling by a reconstituted TMEM16 ion channel. *Nat. Commun.* 4:2367. https://doi.org/10.1038/ncomms3367

McWilliam, H., W. Li, M. Uludag, S. Squizzato, Y.M. Park, N. Buso, A.P. Cowley, and R. LopezAnalysis Tool Web Services from the EMBL-EBI. Nucleic Acids Res. 2013: 41(Web Server issue):W597-600.

Mirnikjoo, B., K. Balasubramanian, and A.J. Schroit. 2009. Suicidal membrane repair regulates phosphatidylserine externalization during apoptosis. *J. Biol. Chem.* 284:22512–22516. https://doi.org/10.1074/jbc.C109.022913

Mizuta, K., S. Tsutsumi, H. Inoue, Y. Sakamoto, K. Miyatake, K. Miyawaki, S. Noji, N. Kamata, and M. Itakura. 2007. Molecular characterization of GDD1/TMEM16E, the gene product responsible for autosomal dominant gnathodiaphyseal dysplasia. *Biochem. Biophys. Res. Commun.* 357:126–132. https://doi.org/10.1016/j.bbrc.2007.03.108

Park, S.Y., Y. Yun, J.S. Lim, M.J. Kim, S.Y. Kim, J.E. Kim, and I.S. Kim. 2016. Stabilin-2 modulates the efficiency of myoblast fusion during myogenic differentiation and muscle regeneration. *Nat. Commun.* 7:10871. https://doi.org/10.1038/ncomms10871

Pedemonte, N., and L.J. Galietta. 2014. Structure and function of TMEM16 proteins (anoctamins). *Physiol. Rev.* 94:419–459. https://doi.org/10.1152/physrev.00039.2011

Pelz, T., D.R. Drose, D. Fleck, B. Henkel, T. Ackels, M. Spehr, and E.M. Neuhaus. 2018. An ancestral TMEM16 homolog from Dictyostelium discoideum forms a scramblase. *PLoS One.* 13:e0191219. https://doi.org/10.1371/journal.pone.0191219

Picollo, A., M. Malvezzi, and A. Accardi. 2015. TMEM16 proteins: unknown structure and confusing functions. *J. Mol. Biol.* 427:94–105. https://doi.org/10.1016/j.jmb.2014.09.028

Pomorski, T., and A.K. Menon. 2006. Lipid flippases and their biological functions. *Cell. Mol. Life Sci.* 63:2908–2921. https://doi.org/10.1007/s00018-006-6167-7

Pont-Kingdon, G. 1997. Creation of chimeric junctions, deletions, and insertions by PCR. *Methods Mol. Biol.* 67:167–172.

Sancak, Y., T.R. Peterson, Y.D. Shaul, R.A. Lindquist, C.C. Thoreen, L. Bar-Peled, and D.M. Sabatini. 2008. The Rag GTPases bind raptor and mediate amino acid signaling to mTORC1. *Science.* 320:1496–1501. https://doi.org/10.1126/science.1157535

Sarbassov, D.D., D.A. Guertin, S.M. Ali, and D.M. Sabatini. 2005. Phosphorylation and regulation of Akt/PKB by the rictor-mTOR complex. *Science.* 307:1098–1101. https://doi.org/10.1126/science.1106148

Schroeder, B.C., T. Cheng, Y.N. Jan, and L.Y. Jan. 2008. Expression cloning of TMEM16A as a calcium-activated chloride channel subunit. *Cell.* 134:1019–1029. https://doi.org/10.1016/j.cell.2008.09.003

Sims, P.J., T. Wiedmer, C.T. Esmon, H.J. Weiss, and S.J. Shattil. 1989. Assembly of the platelet prothrombinase complex is linked to vesiculation of the platelet plasma membrane. Studies in Scott syndrome: an isolated defect in platelet procoagulant activity. *J. Biol. Chem.* 264:17049–17057.

Sui, T., L. Xu, Y.S. Lau, D. Liu, T. Liu, Y. Gao, L. Lai, R. Han, and Z. Li. 2018. Development of muscular dystrophy in a CRISPR-engineered mutant rabbit model with frame-disrupting ANO5 mutations. *Cell Death Dis.* 9:609. https://doi.org/10.1038/s41419-018-0674-y

Suzuki, J., M. Umeda, P.J. Sims, and S. Nagata. 2010. Calcium-dependent phospholipid scrambling by TMEM16F. *Nature.* 468:834–838. https://doi.org/10.1038/nature09583

Suzuki, J., T. Fujii, T. Imao, K. Ishihara, H. Kuba, and S. Nagata. 2013. Calcium-dependent phospholipid scramblase activity of TMEM16 protein family members. *J. Biol. Chem.* 288:13305–13316. https://doi.org/10.1074/jbc.M113.457937

van den Eijnde, S.M., A.J. Luijsterburg, L. Boshart, C.I. De Zeeuw, J.H. van Dierendonck, C.P. Reutelingsperger, and C. Vermeij-Keers. 1997. In situ detection of apoptosis during embryogenesis with annexin V: from whole mount to ultrastructure. *Cytometry.* 29:313–320. https://doi.org/10.1002/(SICI)1097-0320(19971201)29:4%3C313::AID-CYTO8%3E3.0.CO;2-A

van den Eijnde, S.M., M.J. van den Hoff, C.P. Reutelingsperger, W.L. van Heerde, M.E. Henfling, C. Vermeij-Keers, B. Schutte, M. Borgers, and F.C. Ramaekers. 2001. Transient expression of phosphatidylserine at cell-cell contact areas is required for myotube formation. *J. Cell Sci.* 114:3631–3642.

van Meer, G., D.R. Voelker, and G.W. Feigenson. 2008. Membrane lipids: where they are and how they behave. *Nat. Rev. Mol. Cell Biol.* 9:112–124. https://doi.org/10.1038/nrm2330

Whitlock, J.M., and H.C. Hartzell. 2016. A Pore Idea: the ion conduction pathway of TMEM16/ANO proteins is composed partly of lipid. *Pflugers Arch.* 468:455–473. https://doi.org/10.1007/s00424-015-1777-2

Whitlock, J.M., and H.C. Hartzell. 2017. Anoctamins/TMEM16 Proteins: Chloride Channels Flirting with Lipids and Extracellular Vesicles. *Annu. Rev. Physiol.* 79:119–143. https://doi.org/10.1146/annurev-physiol-022516-034031

Whitlock, J.M., K. Yu, Y.Y. Cui, D. Griffin, L. Rodino-Klapac, and H.C. Hartzell. 2015. The role of TMEM16E/Anoctamin 5 in muscular dystrophy and phospholipid scramlbing. *J. Gen. Physiol.* 146:16A–16A.

Whitlock, J.M., K. Yu, Y.Y. Cui, and H.C. Hartzell. 2016. Limb-girdle muscular dystrophy 2L is caused by a defect in phospholipid scrambling mediated by ANO5. *J. Gen. Physiol.* 148:35A.

Xu, J., M. El Refaey, L. Xu, L. Zhao, Y. Gao, K. Floyd, T. Karaze, P.M. Janssen, and R. Han. 2015. Genetic disruption of Ano5 in mice does not recapitulate human ANO5-deficient muscular dystrophy. *Skelet. Muscle.* 5:43. https://doi.org/10.1186/s13395-015-0069-z

Xu, J., L. Xu, Y.S. Lau, Y. Gao, S.A. Moore, and R. Han. 2018. A novel ANO5 splicing variant in a LGMD2L patient leads to production of a truncated aggregation-prone Ano5 peptide. *J. Pathol. Clin. Res.* 4:135–145. https://doi.org/10.1002/cjp2.92

Yang, Y.D., H. Cho, J.Y. Koo, M.H. Tak, Y. Cho, W.S. Shim, S.P. Park, J. Lee, B. Lee, B.M. Kim, et al. 2008. TMEM16A confers receptor-activated calcium-dependent chloride conductance. *Nature.* 455:1210–1215. https://doi.org/10.1038/nature07313

Yu, K., C. Duran, Z. Qu, Y.Y. Cui, and H.C. Hartzell. 2012. Explaining calcium-dependent gating of anoctamin-1 chloride channels requires a revised topology. *Circ. Res.* 110:990–999. https://doi.org/10.1161/CIRCRESAHA.112.264440

Yu, K., J.M. Whitlock, K. Lee, E.A. Ortlund, Y.Y. Cui, and H.C. Hartzell. 2015. Identification of a lipid scrambling domain in ANO6/TMEM16F. *eLife.* 4:e06901. https://doi.org/10.7554/eLife.06901

Zaitseva, E., E. Zaitsev, K. Melikov, A. Arakelyan, M. Marin, R. Villasmil, L.B. Margolis, G.B. Melikyan, and L.V. Chernomordik. 2017. Fusion Stage of HIV-1 Entry Depends on Virus-Induced Cell Surface Exposure of Phosphatidylserine. *Cell Host Microbe.* 22:99–110.e7. https://doi.org/10.1016/j.chom.2017.06.012